LUMINESCENCE MEASUREMENTS OF Xe^+ + N_2 AND Xe^{2+} + N_2 HYPERTHERMAL CHARGE TRANSFER COLLISIONS (POSTPRINT)

Benjamin D. Prince and Yu-Hui Chiu

10 April 2012

Interim Report

AIR FORCE RESEARCH LABORATORY
Space Vehicles Directorate
3550 Aberdeen Ave SE
AIR FORCE MATERIEL COMMAND
KIRTLAND AIR FORCE BASE, NM 87117-5776

DTIC COPY

NOTICE AND SIGNATURE PAGE

Using Government drawings, specifications, or other data included in this document for any purpose other than Government procurement does not in any way obligate the U.S. Government. The fact that the Government formulated or supplied the drawings, specifications, or other data does not license the holder or any other person or corporation; or convey any rights or permission to manufacture, use, or sell any patented invention that may relate to them.

This report was cleared for public release by the Air Force Research Laboratory 377 ABW Public Affairs Office and is available to the general public, including foreign nationals. Copies may be obtained from the Defense Technical Information Center (DTIC) (http://www.dtic.mil).

AFRL-RV-PS-TR-2012-0093 HAS BEEN REVIEWED AND IS APPROVED FOR PUBLICATION IN ACCORDANCE WITH ASSIGNED DISTRIBUTION STATEMENT.

//signed//   //signed//

_____   _____
Raymond Bemish, RVBXT   Joel Mozer, PhD
Project Manager   Chief, AFRL/RVB

This report is published in the interest of scientific and technical information exchange, and its publication does not constitute the Government's approval or disapproval of its ideas or findings.

REPORT DOCUMENTATION PAGE

Form Approved
OMB No. 0704-0188

1. REPORT DATE *(DD-MM-YYYY)* 10-04-2012	2. REPORT TYPE Interim Report	3. DATES COVERED *(From - To)* 1 Oct 2010 to 30 Sep 2011

4. TITLE AND SUBTITLE

LUMINESCENCE MEASUREMENTS OF $Xe^+ + N_2$ AND $Xe^{2+} + N_2$ HYPERTHERMAL CHARGE TRANSFER COLLISIONS (POSTPRINT)

5a. CONTRACT NUMBER

5b. GRANT NUMBER

5c. PROGRAM ELEMENT NUMBER 61102F

6. AUTHOR(S)

Benjamin D. Prince and Yu-Hui Chiu

5d. PROJECT NUMBER 2301

5e. TASK NUMBER PPM00004270

5f. WORK UNIT NUMBER EF004373

7. PERFORMING ORGANIZATION NAME(S) AND ADDRESS(ES)

Air Force Research Laboratory
Space Vehicles Directorate
3550 Aberdeen Ave SE
Kirtland AFB, NM 87117-5776

8. PERFORMING ORGANIZATION REPORT NUMBER

AFRL-RV-PS-TR-2012-0093

9. SPONSORING / MONITORING AGENCY NAME(S) AND ADDRESS(ES)

10. SPONSOR/MONITOR'S ACRONYM(S) AFRL/RVBXT

11. SPONSOR/MONITOR'S REPORT NUMBER(S)

12. DISTRIBUTION / AVAILABILITY STATEMENT

Approved for public release. Distribution is unlimited. (377ABW-2011-0792 dtd 6 Jun 2011)

13. SUPPLEMENTARY NOTES
THE JOURNAL OF CHEMICAL PHYSICS 135, 104308 (2011). Government Purpose Rights.

14. ABSTRACT

Luminescence spectra are recorded for collisions between Xe^+/Xe^{2+} and molecular nitrogen at energies ranging from 4.5 to 316 eV in the center-of-mass frame. In the $Xe^+ + N_2$ collision system, evidence for luminescent charge-transfer products is only found through Xe I emission lines. The most intense features of the luminescence spectra are attributed to atomic N emissions observed above ~20 eV. Intense N_2^+ A $^2\Pi_u - X\ ^2\Sigma_g^+$ and B $^2\Sigma_u^+ - X\ ^2\Sigma_g^+$ radiance is observed from $Xe^{2+} + N_2$ collisions. The B state formation cross section decreases with collision energy until 20 eV, after which it becomes independent of impact energy with an approximate value of 3 Å^2. The cross section for N_2^+ A (v > 0) formation increases with energy until 20 eV, after which it remains nearly constant at ~1 Å^2. The N_2^+ product vibrational distributions extracted from the spectra are non-Franck-Condon for both electronic product states at low collision energies. The distributions resemble a Franck-Condon distribution at the highest energies investigated in this work

15. SUBJECT TERMS
charge exchange, Franck-Condon factors, ion-molecule collisions, luminescence, nitrogen, positive ions, vibrational states, xenon

16. SECURITY CLASSIFICATION OF:

c. REPORT Unclassified	b. ABSTRACT Unclassified	c. THIS PAGE Unclassified

17. LIMITATION OF ABSTRACT Unlimited

18. NUMBER OF PAGES 14

19a. NAME OF RESPONSIBLE PERSON Raymond Bemish

19b. TELEPHONE NUMBER *(include area code)*

Standard Form 298 (Rev. 8-98)
Prescribed by ANSI Std. 239.18

Luminescence measurements of Xe$^+$ + N$_2$ and Xe^{2+} + N$_2$ hyperthermal charge transfer collisions

Benjamin D. Prince and Yu-Hui Chiu[a)]
Air Force Research Laboratory, Space Vehicles Directorates, Hanscom AFB, Massachusetts 01731, USA

Luminescence spectra are recorded for collisions between Xe$^+$/Xe^{2+} and molecular nitrogen at energies ranging from 4.5 to 316 eV in the center-of-mass frame. In the Xe$^+$ + N$_2$ collision system, evidence for luminescent charge-transfer products is only found through Xe I emission lines. The most intense features of the luminescence spectra are attributed to atomic N emissions observed above ∼20 eV. Intense N$_2^+$ A $^2\Pi_u$ − X $^2\Sigma_g^+$ and B $^2\Sigma_u^+$ − X $^2\Sigma_g^+$ radiance is observed from Xe^{2+} + N$_2$ collisions. The B state formation cross section decreases with collision energy until 20 eV, after which it becomes independent of impact energy with an approximate value of 3 Å^2. The cross section for N$_2^+$ A ($v > 0$) formation increases with energy until 20 eV, after which it remains nearly constant at ∼1 Å^2. The N$_2^+$ product vibrational distributions extracted from the spectra are non-Franck-Condon for both electronic product states at low collision energies. The distributions resemble a Franck-Condon distribution at the highest energies investigated in this work. [doi:10.1063/1.3629453]

I. INTRODUCTION

The reactions of rare gas ions with molecular nitrogen have garnered significant experimental and theoretical attention over the past few decades and have represented a theoretical benchmark for ion-molecule charge-transfer (CT) dynamics.[1–4] Ion-molecule reactions offer significant advantages in terms of translational and electronic energy control. These advantages have resulted in fundamental insights into how non-adiabatic effects manifest themselves in vibrational state-to-state dynamics.[5,6] The study of ion-molecule chemiluminescence has been especially useful in deriving information on the state-to-state dynamics of hyperthermal ion-molecule collision systems, in particular product state distributions.[7–9] In the present work, we examine luminescence spectra observed in hyperthermal Xe$^+$/Xe^{2+} + N$_2$ collisions.

The energetics associated with charge transfer dictates the dynamics of most hyperthermal ion-molecule collision systems including the reactions of rare-gas (Rg) ions with nitrogen. For the exothermic Rg$^+$ + N$_2$ charge-transfer systems, charge transfer dominates the dynamics including reactive processes. The charge-transfer state-to-state dynamics are governed by energy resonance and Franck-Condon (FC) criteria.[10,11] Energy resonance signifies a propensity to produce product states with asymptotic energies close or equal to the reactant states, which is symptomatic of long-range dynamics. Franck-Condon criteria are based on the need for significant overlap between reactant and product vibrational wavefunctions. Consequently, the general trend at low collision energies is to observe near resonant charge-transfer product states with significant Franck-Condon overlap, provided

there is significant coupling between reactant and product electronic states. With increasing collision energies, the growing non-adiabaticity results in a broadening of the vibrational product state distributions. At the high energy limit, a Franck-Condon distribution is expected.

In the charge-transfer reaction of Ar$^+$ + N$_2$, the most populated vibrational state at low collision energies was found theoretically and experimentally to be N$_2^+$ (X, $v = 1$) due to the near energy resonance of the product and reactant channels.[3,12,13] This state preference decreases as collision energy increases and is predicted to eventually lead to a FC distribution with preference of $v = 0$ at high collision energy limit. Similarly, reaction of He$^+$ + N$_2$ at near-thermal energies found that the nearly resonant He (^{1}S) + N$_2^+$ (C$^2\Pi_u^+$, $v = 3$) products are approximately 60 times more populated than the exothermic CT reaction to N$_2^+$ (B, $^2\Sigma_u^+$).[2] Generally, for these well-studied exothermic Rg$^+$ (Ar$^+$, He$^+$, and Ne$^+$) + N$_2$ systems, the energy resonance and FC criteria are effective in predicting the resulting product states at low collision energies. In contrast, the dynamics of Xe$^+$ + N$_2$ are expected to differ due to the lack of energy resonance in this highly endothermic system (process 1 below). As a consequence, the resulting products are expected to be formed largely from collisions with significant translational energy transfer.

The exothermic doubly charged Xe^{2+} + N$_2$ charge-transfer system exhibits a thermal rate constant near the Langevin value as determined by Adams *et al.* for the ground and first metastable state of Xe^{2+}.[14] Doubly charged ion charge-transfer systems are known to follow long-range dynamics associated with an efficient curve-crossing mechanism involving the long-range attractive ion-induced dipole potentials of the reactants and the repulsive Coulomb potentials of the ionic products.[14–17] These previous works have highlighted the importance of the "reaction window" model, where optimal CT occurs for crossings at interatomic

---
[a)]Current address: Busek Company, Inc., 11 Tech Circle, Natick, MA 01760. Electronic mail: ychiu@busek.com.
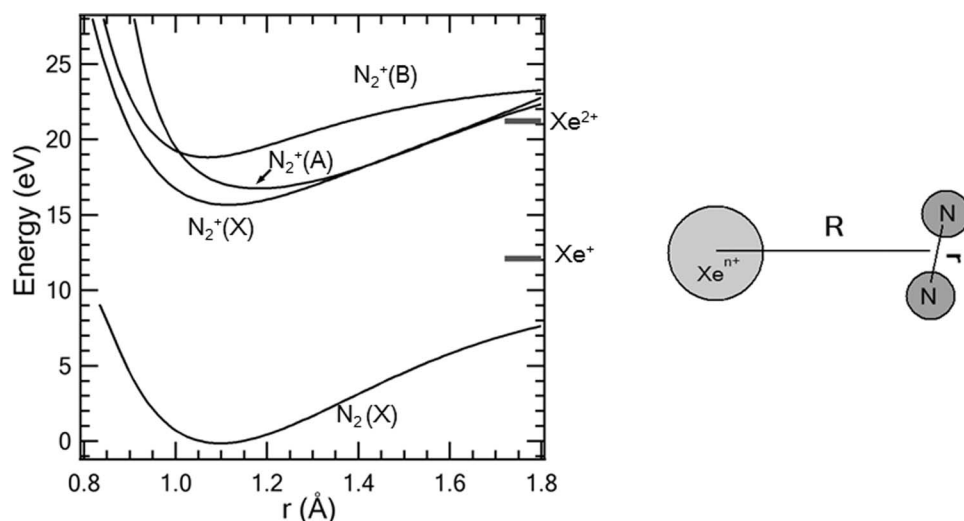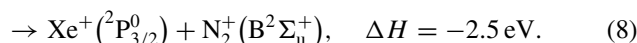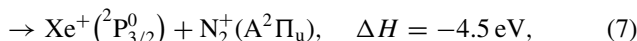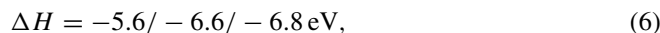
FIG. 1. Left: Asymptotic potential curves for N_2 and N_2^+ and energy levels of Xe ions relevant to the charge-transfer reactions. Right: Collision model depicting the two relevant distances—R, the internuclear distance between the Xe ions and N_2 and r, the N_2 bond length.

distances between 2 and 6 Å.[15] This is consistent with Landau-Zener curve-crossing models,[18] where CT probabilities are maximum at intermediate coupling distances. Lindinger[16] studied charge-transfer rate coefficients of Ar^{2+} with a variety of atoms and determined that rate coefficients peaked for systems with crossing near 4 Å. Unlike the exothermic singly charged charge-transfer systems, product state distributions do not follow energy resonance criteria and are instead associated with the vibronic states undergoing favorable curve-crossings which have significant exothermic energy gaps due to the high long range Coulomb potential at the crossings. At 4 Å, the Coulomb energy is 3.6 eV. Doubly charged systems, similar to the singly charged counterparts, have been found to produce vibrational populations resembling FC distributions in the high energy limit.[19]

In the present work, we report $Xe^{n+} + N_2$, n = 1, 2, luminescence studies over collision energies ranging from 4.5 to 316 eV in the center-of-mass frame (E_{cm}). As in other rare gas ion reactions with molecules, the dynam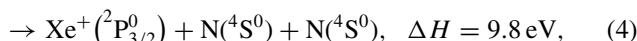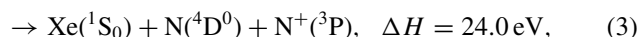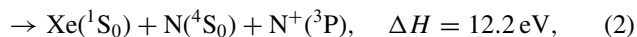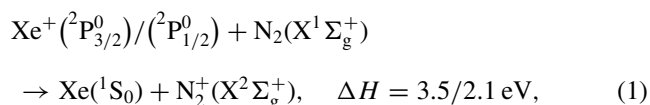ics are governed by the energetics of charge-transfer reactions. Figure 1 displays asymptotic potentials along the N-N coordinate on an energy scale referenced with respect to neutral xenon and nitrogen. The ionization energy of N_2 is 15.581 eV, while the ionization energies of Xe and Xe^+ are 12.1 and 21.2 eV, respectively. Thus, the $Xe^+ + N_2$ charge-transfer system is considerably endothermic, while the $Xe^{2+} + N_2$ single-electron transfer reaction can access the $X\,^2\Sigma_g^+$, $A\,^2\Pi_u$, and $B\,^2\Sigma_u^+$ states of N_2^+ exothermically. The energetics of several possible product channels for the reactions of Xe^+ and Xe^{2+} with N_2 are listed below for the ground and spin-orbit excited state Xe^{n+} species, including products of CT processes (1, 6-8), dissociative charge-transfer (DCT) processes (2 and 3), and collision induced dissociation (CID) pathways (4 and 5):

$$Xe^+\left(^2P_{3/2}^0\right)/\left(^2P_{1/2}^0\right) + N_2(X\,^1\Sigma_g^+)$$

$$\rightarrow Xe(^1S_0) + N_2^+(X\,^2\Sigma_g^+), \quad \Delta H = 3.5/2.1\,\text{eV}, \quad (1)$$

$$\rightarrow Xe(^1S_0) + N(^4S^0) + N^+(^3P), \quad \Delta H = 12.2\,\text{eV}, \quad (2)$$

$$\rightarrow Xe(^1S_0) + N(^4D^0) + N^+(^3P), \quad \Delta H = 24.0\,\text{eV}, \quad (3)$$

$$\rightarrow Xe^+\left(^2P_{3/2}^0\right) + N(^4S^0) + N(^4S^0), \quad \Delta H = 9.8\,\text{eV}, \quad (4)$$

$$\rightarrow Xe^+\left(^2P_{3/2}^0\right) + N(^4D^0) + N(^4S^0), \quad \Delta H = 21.6\,\text{eV}, \quad (5)$$

$$Xe^{2+}(^3P_2)/(^3P_1)/(^3P_0) + N_2\left(X\,^1\Sigma_g^+\right)$$

$$\rightarrow Xe^+\left(^2P_{3/2}^0\right) + N_2^+\left(X\,^2\Sigma_g^+\right),$$

$$\Delta H = -5.6/-6.6/-6.8\,\text{eV}, \quad (6)$$

$$\rightarrow Xe^+\left(^2P_{3/2}^0\right) + N_2^+(A\,^2\Pi_u), \quad \Delta H = -4.5\,\text{eV}, \quad (7)$$

$$\rightarrow Xe^+\left(^2P_{3/2}^0\right) + N_2^+(B\,^2\Sigma_u^+), \quad \Delta H = -2.5\,\text{eV}. \quad (8)$$
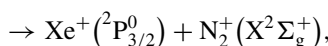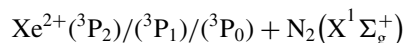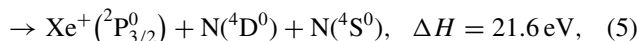
In this paper, we compare the luminescence results of the endothermic $Xe^+ + N_2$ system with the exothermic reaction of $Xe^{2+} + N_2$ system over a wide collision energy range. Figure 1 and the $Xe^{2+} + N_2$ energetics demonstrate that this system can produce two electronically excited states of the nitrogen ion that are known to radiate with high Einstein A coefficients. Thus, this system offers a unique opportunity to examine the change in state-to-state CT dynamics as the translational non-adiabaticity increases with collision energy. In Sec. II, we detail the spectral analyses used to derive the vibrational populations of the N_2^+ products as well as the procedure for converting the measured luminescence spectra into absolute excitation cross sections. In Sec. III, the luminescence results of the $Xe^{n+} + N_2$ collision systems are presented along with the results extracted from simulations. The results are interpreted in Sec. IV.

II. EXPERIMENT

All experimental measurements were performed using an ion beam-cell luminescence apparatus.[20] This apparatus has been described previously and a brief summary is given here.

A glow discharge ion source generates a xenon ion beam which is directed into a Wien velocity filter that allows for selection of the ion mass and charge (Xe^+ or Xe^{2+} in this case). Typical anode voltages are 25 V and 100 V for Xe^+ and Xe^{2+}, respectively. Based on the anode voltages used in the discharge source, statistical distributions of spin-orbit states composed of Xe^+ ($^2P^0_{3/2}$ and $^2P^0_{1/2}$) and Xe^{2+} ($^3P_2$, $^3P_1$, and $^3P_0$) are assumed, respectively. The ion beam is then focused into a collision cell filled with the target gas at a set pressure. After passing through the collision cell, the ion beam current is measured by a Faraday cup and the divergence of the beam is determined by additionally measuring the current registered on the back wall of the collision cell. The total beam current is taken to be the sum of both measured values. To measure the ion beam energy, a retarding potential analyzer is used that consists of high transmittance gold grids placed in front of the Faraday cup. An applied voltage is ramped and the Faraday cup current is monitored. The first derivative of the current versus applied voltage provides the beam energy distribution. The pressure of the nitrogen target gas (Matheson, 99.995%) is held at a cell pressure of 1.5 mTorr and is monitored by a capacitance manometer. Both the pressure and beam currents are continuously monitored during the experiment, and the time averaged values are used for analysis.

The luminescence is collected using a fiber optic bundle that is coupled to the collision cell. The light emission is dispersed via a spectrometer (Shamrock 303i, Andor Technology) and detected by a CCD detector (IDus DU-420, Andor Technology). The experimental resolution of 0.75–0.85 nm, determined by measuring the full width at half maximum of xenon atomic lines, is obtained with a 600 line per mm grating and slit width of 200 μm. The wavelength scale is calibrated by using known Xe neutral and Xe^+ lines as well as atomic N lines when present. To acquire accurate chemiluminescent cross sections, the spectral sensitivity of the spectrograph must be determined. A spectral sensitivity curve was obtained from the black-body spectrum of a calibrated halogen-tungsten lamp. The resulting calibration curve is consistent with the specifications of the CCD sensitivity, grating efficiency, and fiber optic transmission curve. Because of this consistency, we adopted the specifications for the ultraviolet (UV) spectral sensitivity for $\lambda < 380$ nm. As a result, the experimental uncertainties of the cross section values are higher for states radiating in the UV. The absolute excitation cross sections are determined by the method described previously[20] using the following equation:

$$\sigma_\lambda = \frac{qeJ_\lambda}{GPI}, \qquad (9)$$

where q is the charge of the colliding ion, e is the electronic charge, J_λ is the intensity in photons per unit time integrated over the entire spectral width of a given line, P is the target gas pressure, and I is the total beam current. G, the geometry factor, is determined from reproducing previously known emission excitation cross sections.[20,21] The uncertainty of the experiment is estimated to be 30% and 40% for the visible-near-infrared and UV regions, respectively. The relative cross section uncertainty from run-to-run is generally within 5%.

To determine emission excitation cross sections for specific molecular bands associated with a specific vibrational transition within an electronic manifold of transitions, and to derive nascent product state populations, spectral simulations are conducted using the software package DIATOMIC.[22] These simulations consisted of generating a basis set of individual functions for each vibrational transition observed in the spectra. Molecular constants for N_2^+ and its excited states were obtained from several sources.[23–25] The best fit coefficients were then used to determine the population of each upper state in an electronic band using the following equation:[26]

$$P(v') = \frac{Z\lambda^4_{v',v''}}{FR_e^2 q_{v',v''}}, \qquad (10)$$

where $P(v')$ is the population of the emitting vibrational state, Z is the best fit basis coefficient, F is a proportionality constant that is identical for all transitions in an electronic band, $\lambda_{v',v''}$ is the wavelength of the emission in nm, R_e is the average electronic transition moment, and $q_{v',v''}$ is the Franck-Condon factor for the transitions (v',v''). The R_e and $q_{v',v''}$ values used are taken from Gilmore, Lahey, and Espy.[27] To determine the populations, the $P(v')$ and F parameters were varied to minimize the difference between the predicted Z and best fit Z, subject to the constraint that the sum of the populations of the emitting states of an electronic state equals unity and that only one F factor could be employed for the analysis.

III. RESULTS

Luminescence measurements have been performed for the $Xe^+ + N_2$ reaction over a collision energy range between $E_{cm} = 4.4$ and 211 eV. The only emissions observed in the 280–1000 nm range were assigned to excited xenon neutral (Xe I) and atomic nitrogen (N I). An example spectrum at 211 eV is presented in Fig. 2(a). At high collision energies, emissions from excited Xe^+ (Xe II) can be observed in the 400–550 nm range and, for collision energies greater than 50 eV, prominent Xe I lines are observed throughout the near infrared (NIR) region. Figure 2(b) compares a $Xe^+ + N_2$ spectrum at 211 eV to a scaled $Xe^+ + Xe$ luminescence spectrum at 150 eV. The $Xe^+ + Xe$ luminescence spectrum[20,21] contains prominent Xe I and Xe II lines that are also observed in the present system and are used to contrast the lines that result from nitrogen emissions in the NIR. Several strong lines are observed, some of which are well isolated from the xenon lines that dominate the region. Lines from 855–872 nm and 818–823 nm can be assigned to the $3p \rightarrow 3s$ transitions of various states of atomic nitrogen. Similarly, Fig. 2(c) compares a $Xe^+ + N_2$ spectrum at 211 eV to a scaled $Xe^+ + Xe$ luminescence spectrum at 150 eV for the visible spectral range. A group of atomic nitrogen lines is located primarily between 745 and 750 nm. Atomic nitrogen lines from various upper states including $^4S^0$, ^2P, $^4P^0$, $^2P^0$, ^4F, and $^4D^0$ can be identified at high energies and the relevant transitions are listed in Table I.[28] Due to the presence of large numbers of xenon lines and the resolution of these experiments, it is unclear if emissions from N^+ are observed. A peak observed between two atomic xenon lines with wavelength 648.6 nm could be
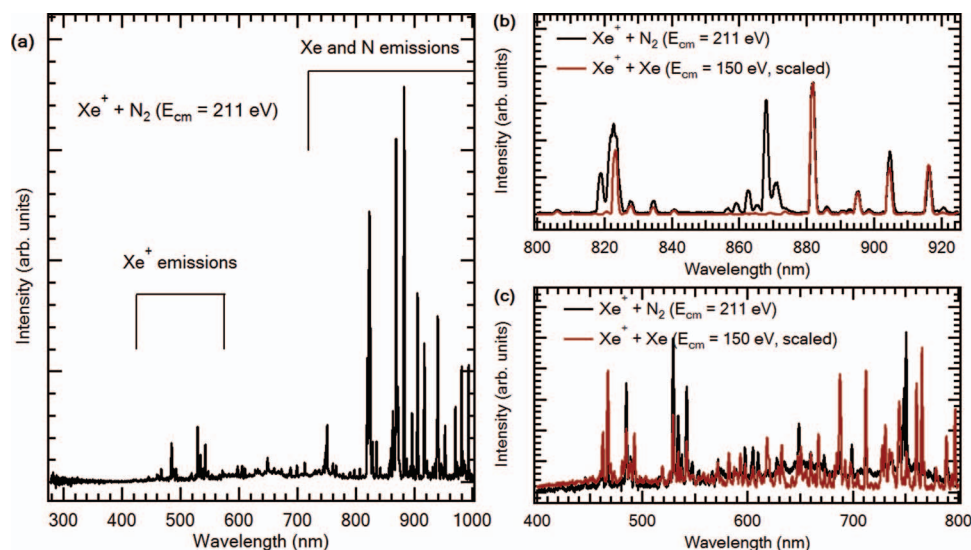
FIG. 2. (a) Chemiluminescence spectrum obtained for $Xe^+ + N_2$ at 211 eV. (b) Expanded view of the 800-925 nm range. Atomic N lines are observed near 820 and 870 nm. (c) Expanded view in the 400–800 nm region where additional N emissions are observed near 750 nm.

assigned to a known $N^+(^1P \rightarrow {}^1P^0)$ transition at 648.2 nm, but could also be assigned to one of the five N transitions from 648.17 to 649.12 nm. The cross section energy dependence for the excitation of the most intense neutral xenon 881.9 nm line $(6s^2[3/2]^0\text{-}6p^2[5/2])$ and a cluster of N I lines (854–873 nm) is plotted as a function of collision energy in Fig. 3. The cross sections increase with collision energy and exhibit an onset around 20 eV.

Figure 4(a) shows luminescence spectra over a broad spectral range for the $Xe^{2+} + N_2$ collision system at 316 eV and 17.6 eV, respectively. Both N_2^+ (B-X) and N_2^+ (A-X) bands are observed. N I emissions are observed at high collision energies but the emissions are weak compared to the charge-transfer N_2^+ luminescence contribution. Apart from the N I intensities and the signal-to-noise (S/N) ratio, which falls as the ion beam energy decreases due to reduction of the total ion current, the differences between the two spectra observed at different energies are minor. Xe II lines become

more prevalent as the beam energy is increased and their intensity appears to be a linear function of beam energy (not shown). At the highest sampled energies, Xe I lines are also observed.

The N_2^+ B-X bands are significantly stronger than the A-X bands. In Figs. 4(a) and 4(b), the most intense band at 391 nm is truncated for better comparison of the weaker bands. Significant second-order diffraction signal, labeled with asterisks, is seen for the strongest B-X bands in spectral regions of the A-X bands. Vibrational band assignments for the N_2^+ (B-X) are indicated in Fig. 4(b), where the most intense band is attributable to the $\Delta v = 0$ vibrational band sequence. Δv refers to the difference in the vibrational quantum number of upper and lower states $(v' - v'')$ in the N_2^+ (B, $v' \rightarrow$ X, v'') transition. It is also found that for $\Delta v < 0$ transitions, the most intense bands originate from the excited $v = 0$ states. The $\Delta v > 0$ transitions contain overlapping bands which are unresolved, given the experimental resolution, but can be deconvoluted through the spectral simulations. The A-X vibrational transitions in Fig. 4(c) are com-

TABLE I. Assignments of N I transitions observed in $Xe^+ + N_2$ collisions and their energies with respect to the N I ground state.

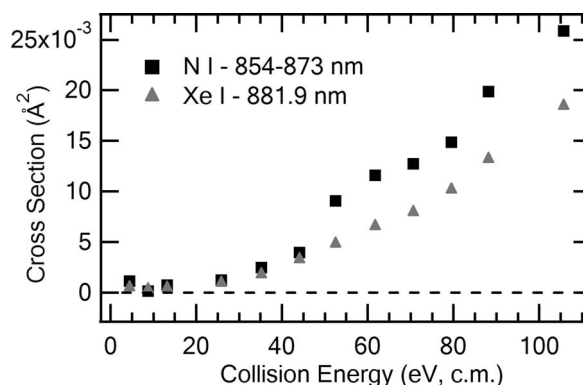| Wavelength (nm)	Upper state	Transition	Upper state energy (eV)
939	$^2D^0$	^2P–$^2D^0$	12.0
871	$^4D^0$	^4P–$^4D^0$	11.8
868	$^4D^0$	^4P–$^4D^0$	11.8
865	$^2P^0$	^2D–$^2P^0$	12.1
863	$^2P^0$	^2P–$^2P^0$	12.1
859	$^2P^0$	^2P–$^2P^0$	12.1
857	$^2P^0$	^2P–$^2P^0$	12.1
823	$^4P^0$	^4P–$^4P^0$	11.8
819	$^4P^0$	^4P–$^4P^0$	11.8
750	^2P	$^2D^0$–^2P	13.7
748	^2P	$^2D^0$–^2P	13.7
747	$^4S^0$	^4P–$^4S^0$	12.0
649	^4F	$^4D^0$–^4F	13.7

FIG. 3. Energy dependence of the emission excitation cross section of the Xe I 881.9 nm line (filled triangles) and the NI band integrated between 854 and 873 nm (filled squares).
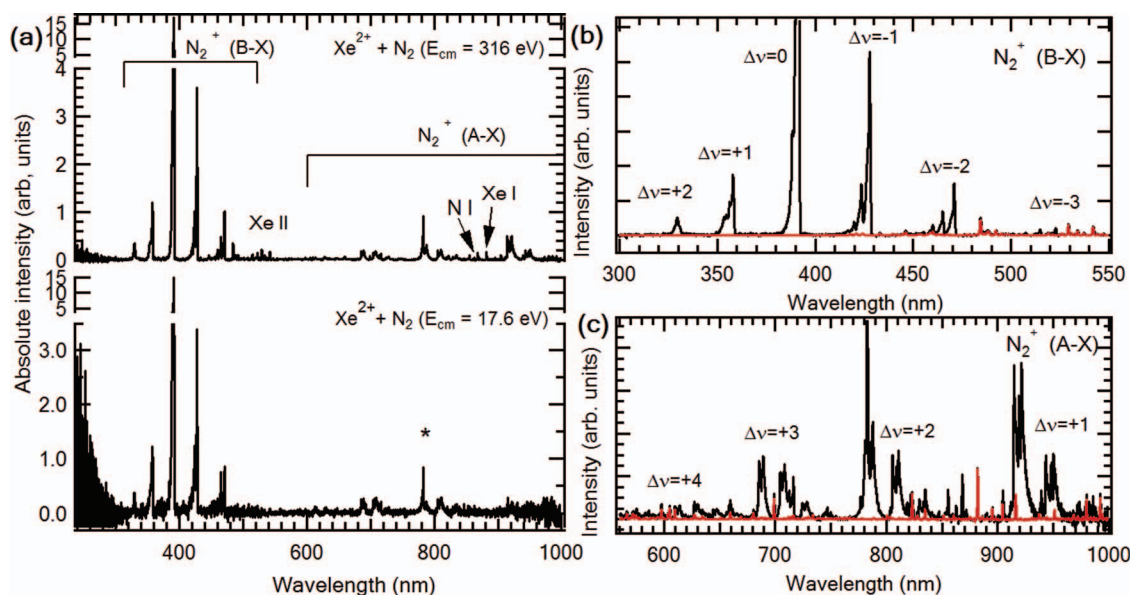
Approved for public release. Distribution is unlimited.

FIG. 4. (a) $Xe^{2+} + N_2$ luminescence spectra at 17.6 and 316 eV, respectively. The asterisk denotes the second-order diffraction of the 391 nm peak at 782 nm. (b) Expanded view of the N_2^+(B-X) region between 300 and 550 nm observed at 316 eV (black) with a scaled Xe^{2+} + Xe spectrum at 300 eV (red). (c) Expanded view of the N_2^+(A-X) region between 560 and 1000 nm observed at 316 eV (black) with a scaled Xe^{2+} + Xe spectrum at 300 eV (red).

pletely resolved. Due to the significant spin-orbit coupling, each transition has two band heads at this resolution. Only $\Delta v > 0$ transitions can be detected, as the $\Delta v = 0$ and $\Delta v < 0$ transitions are at wavelengths where the detection system used has extremely low sensitivity.

The most intense A-X band observed is the 1-0 band at 920 nm. Figure 4(a) demonstrates that, as beam energy decreases, the relative intensity of the A-X 1-0 band near 920 nm significantly diminishes, while the intensities of the other bands appear unchanged. When simulating the A-X bands, it was found that a rotational temperature of 300 K, the experimental temperature of the target nitrogen gas, best described the rotational envelopes of all bands. To minimize the contributions due to Xe I lines in the spectrum, a scaled Xe^{2+} + Xe spectrum was first subtracted from the raw spectrum prior to the spectral fitting simulations. Figure 5 shows the
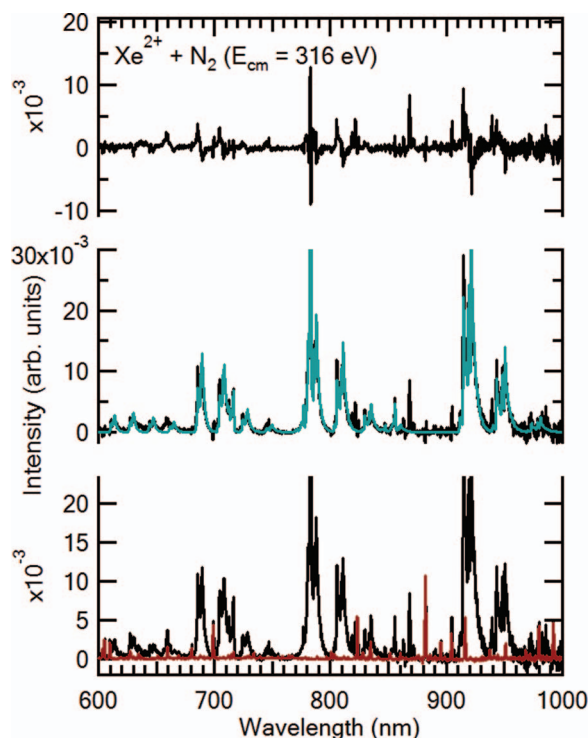

FIG. 5. Bottom: Normalized raw N_2^+ (A-X) luminescence spectrum for $Xe^{2+} + N_2$ at 316 eV (black) with scaled Xe^{2+} + Xe at 300 eV (red). Middle: Normalized spectrum minus Xe scaled spectrum (black) with best simulation fit (teal). Top: Residual after fit.
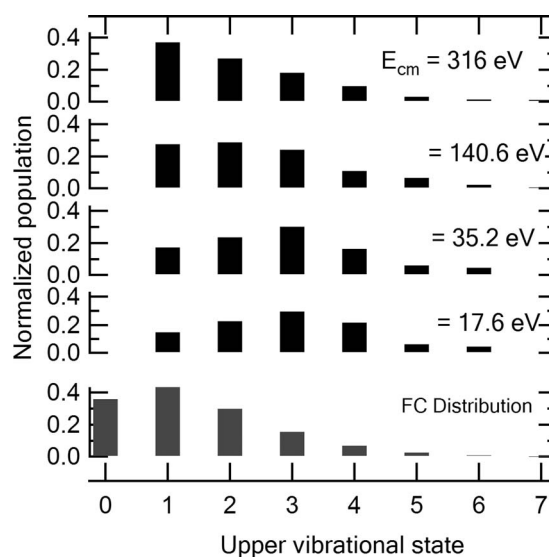
FIG. 6. N_2^+ (A) vibrational state populations derived from the N_2^+ (A-X) spectral analysis at selected energies for $Xe^{2+} + N_2$ collisions. The populations are normalized such that $\Sigma v_i = 1$ for i from 1 to 6. Emissions due to N_2^+ (A, $v = 0$) products could not be observed. The normalized FC distribution for ionizing N_2 (X, $v = 0$) to N_2^+ (A) is shown in the bottom of the figure (gray).

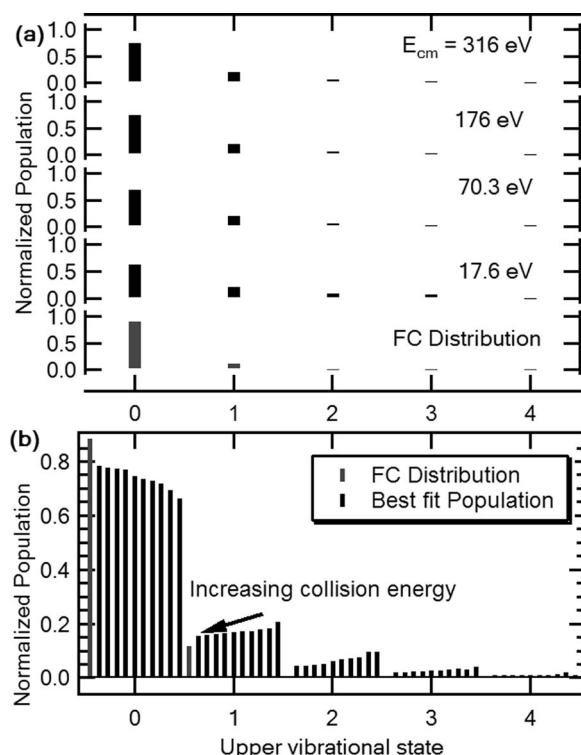Approved for public release. Distribution is unlimited.

FIG. 7. (a) Best fit N_2^+ (B) vibrational state populations derived from the spectral analysis of the N_2^+ (B-X) spectrum at selected energies for Xe^{2+} + N_2 collisions. The predicted FC population is shown in gray. (b) Same as (a) except for all collision energies.

residual resulting from the subtraction process for a luminescence spectrum taken at 316 eV.

Figure 6 shows the normalized $N_2^+(A, v)$ populations derived for selected collision energies along with a Franck-Condon distribution for the ionization of N_2 (X, v = 0) to N_2^+ (A). Note that the normalization did not include the N_2^+ (A, v = 0) state for which a population could not be determined. At low collision energies, the experimental distribution deviates from the predicted FC distribution and has considerable population in v = 3 and 4. At the highest energy of 316 eV, the population distribution is very similar to the FC distribution. As with the A-X bands, a 300 K Boltzmann rotational distribution provided the best agreement with the N_2^+
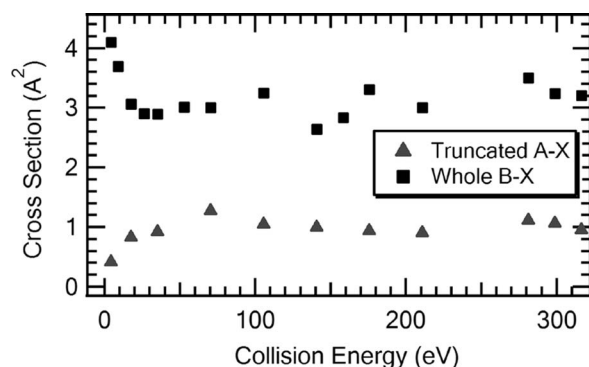

FIG. 8. Comparison of the B-X emission excitation cross section (filled squares) and A-X emission excitation cross section (filled triangles) as a function of collision energy.

TABLE II. Collision energy dependence of N_2^+ (B, $v' \rightarrow$ X, v'' = 0) emission excitation cross sections in 10^{-18} cm^2.

E_{cm}	v' = 0	v' = 1	v' = 2
4.2	176.7	16.2	
17.6	148.6	11.2	1.0
35.2	143.9	10.3	0.9
70.3	158.5	12.0	0.9
105.5	191.3	12.9	0.8
140.6	144.9	9.2	0.8
175.8	170.1	11.5	1.2
210.9	167.4	11.4	0.9
281.2	194.7	13.9	1.1
298.8	179.2	12.6	0.8
316.4	181.3	11.8	1.0

(B-X) data. The derived relative populations are presented in Fig. 7(a). The FC distribution is heavily weighted at N_2^+ (B, v = 0) ≈ 80%. At all collision energies, the relative populations for v > 0 are higher than those of the FC distribution. However, the overall difference with respect to the FC distribution is smaller than in the A-X band. Fig. 7(b) demonstrates that with increasing energy, the N_2^+(B, v) population approaches the FC distribution. Figure 8 plots the integrated emission excitation cross sections for the N_2^+(B-X) and N_2^+(A-X) bands as a function of collision energy. Tables II and III lists the cross sections for respective vibrational levels to N_2^+ (X, v = 0). The B state cross section appears to have a value of ∼3 × 10^{-16} cm^2 over the entire investigated energy range with the exception of the lowest energy value. The entire B-X spectrum is captured in this experiment, unlike for the A-X spectrum. The A state formation cross-section must, therefore, be considered a lower limit since the v = 0 population could not be determined.

IV. DISCUSSION

A. Xe^+ + N_2

The luminescence spectrum of the Xe^+ + N_2 collision system is dominated by emissions from excited Xe I and N I neutral species. The Xe I emissions above 20 eV provide

TABLE III. Collision energy dependence of N_2^+ (A, $v' \rightarrow$ X, v'' = 0) emission excitation cross sections in 10^{-18} cm^2.

E_{cm}	v' = 1	v' = 2	v' = 3	v' = 4
4.2		3.7	5.8	
17.6	8.1	9.0	10.3	2.1
35.2	11.0	9.7	11.3	1.3
70.3	21.4	15.1	12.9	1.2
105.5	21.2	13.1	10.5	2.0
140.6	21.1	12.7	10.0	1.5
175.8	21.7	13.3	9.5	1.1
210.9	25.7	12.1	8.3	1.2
281.2	30.9	15.0	9.1	1.2
298.8	32.4	13.8	7.5	1.2
316.4	28.9	13.5	7.8	1.4

evidence for charge-transfer reactions, either following a non-dissociative (process 1) or dissociative (processes 2 and 3) CT mechanism. Emission from N$_2^+$ (A) or N$_2^+$ (B) was not observed throughout the investigated collision energy range. This does not exclude the possibility of non-dissociative Xe + N$_2^+$(X) products. In a DCT mechanism, formation of N$^+$ would also result in the production of neutral N, which could be the source of the observed N I emissions. Alternatively, N I emissions could also be produced in a CID mechanism (processes 4 and 5). The fact that we see no evidence for N$^+$ emissions suggests that the N I emissions are more likely due to collision-induced dissociation.

The emission excitation cross sections for the transitions with N(^{4}D^0) and N(^{2}P^0) upper states are shown to increase with collision energies above an approximate threshold of 20 eV (see Fig. 3). Excited N(^{4}D^0) atoms can be formed by processes 3 and 5 with thresholds of 24 and 21.6 eV, respectively. The channels leading to N(^{2}P^0) products are nearly isoenergetic with endothermicity only ∼0.3 eV higher. As a result, the thresholds for N(^{4}D^0) and N(^{2}P^0) formation are consistent with the observed N I appearance above 20 eV.

B. Xe^{2+} + N$_2$

For the Xe^{2+} + N$_2$ system, the spectra are dominated by N$_2^+$ A-X and B-X emissions which are clearly a result of single-electron exothermic charge-transfer reactions. For both N$_2^+$ product channels, the derived nascent product vibrational state populations are non-FC at low collision energies and approach a FC distribution with increasing collision energy. The present population analysis points to average internal energies that change a little with collision energy. Furthermore, no evidence is found for rotational excitation of the N$_2^+$ charge-transfer product. Both these observations are evidence for a long range CT mechanism that, in contrast to the Xe$^+$ + N$_2$ system, does not require significant translational energy transfer. This is consistent with thermal experiments by Smith *et al.* who determined that N$_2^+$ was produced with near collisional rates for both the ground ^{3}P and excited ^{1}D$_2$ reactant states of Xe^{2+}.[14] However, at the collision energies investigated in this work, complex formation is negligible and only a direct mechanism needs to be considered. This is confirmed by crossed-beam work by Herman *et al.* of other single-electron transfer processes involving doubly charged ions, where a direct mechanism was an effective event at center-of-mass collision energies below 1 eV.[17,29]

The evolution from a non-FC to a FC product vibrational distribution with collision energy is analogous to the observations made in CT luminescence studies of exothermic reaction systems of singly charged ions.[2,7,10,30] Contrary to the singly charged systems, the N$_2^+$(A) and N$_2^+$(B) product state populations of the present doubly charged systems point to significantly non-resonant processes. This can be attributed to the electron transfer occurring at interatomic distances where the Coulomb interaction of the products is high, resulting in a significant increase in translational energy as the product ions separate. Thermal rate coefficient measurements of doubly charged atomic systems demonstrated that charge transfer is observed, provided a curve crossing between reactant
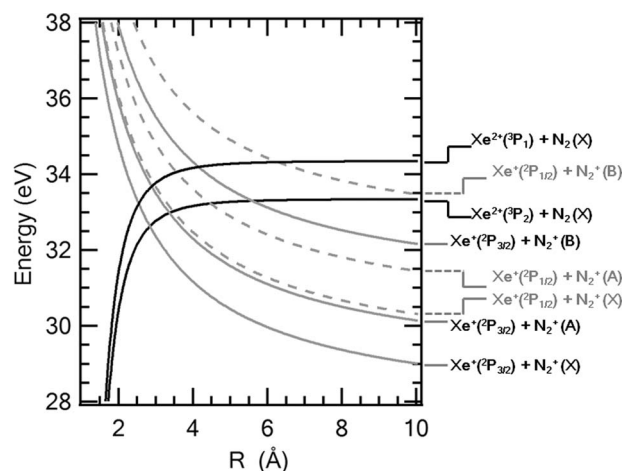

FIG. 9. Interaction potentials of the Xe^{2+}(^{3}P$_{2,1}$) + N$_2$ charge-transfer system. The energy is referenced with respect to the ground state neutrals, Xe + N$_2$. Solid and broken product curves are associated with Xe$^+$ (^{2}P$_{3/2}$) and Xe$^+$ (^{2}P$_{1/2}$) products, respectively.

and product state potentials exists at interatomic distances between 2 and 6 Å. The highest rates for Ar^{2+} collision systems were found where crossings occurred close to 4 Å.[14–16] To assess the role of curve crossings in the present system, we plot in Fig. 9 representative long-range potentials of the rovibronic ground states of the present doubly charge-transfer system. Potentials shown are those for the Coulomb products Xe$^+$(^{2}P$_{3/2,1/2}$) + N$_2^+$ (X,A,B) and the long-range ion-induced dipole potentials of Xe^{2+}(^{2}P$_{2,1}$) + N$_2$(X), V $= -\alpha q^2$ R^{-4}, where α is the isotropic nitrogen polarizability and q is the ion charge. The crossings occur for Xe$^+$(^{2}P$_{3/2}$) + N$_2^+$ products at 5.6 Å (B), 3.38 Å (A), and 2.86 Å (X) and for the Xe$^+$ (^{2}P$_{1/2}$) + N$_2^+$ products at >10 Å (B), 4.52 Å (A), and 3.48 Å (X). Thus, significant charge transfer should be observed for the respective $v = 0$ N$_2^+$ products because all N$_2^+$ electronic state channels have crossings with reactant curves within the relevant window of 2–6 Å. The curves in Fig. 9 make it apparent that no crossing occurs with product states associated with excited xenon ions, which have minimum excitation energy of 11.3 eV.[28] This explains the high N$_2^+$ (A-X) and N$_2^+$ (B-X) intensities in comparison to Xe II emissions. Excited Xe$^+$ ions are, therefore, not likely to be produced by a curve-crossing mechanism.

In order to assess a curve-crossing model for vibrational state-to-state transitions, long-range curve crossings between vibronic potential curves can be examined. Figure 10 shows selected long-range vibronic potentials in the critical coupling window region for both A (a) and B (b) state products. The vibronic curves of the Xe$^+$(^{2}P$_{3/2}$) + N$_2^+$(A, $v = 3,4$) product states cross with Xe^{2+}(^{2}P$_2$) + N$_2$ (X, $v = 0$) reactants close to the commonly quoted maximum coupling distance of 4 Å. This is consistent with the observation of a maximum state-to-state cross section for Xe$^+$(^{2}P$_{3/2}$) + N$_2^+$ (A, $v = 3$) products at low collision energies (see Fig. 6), where the distribution clearly deviates from a FC distribution.

For N$_2^+$ B ($v = 0$) state products produced by ground-state reactants, the shortest crossing occurs at 5.6 Å. This system would, therefore, heavily favor $v = 0$ products be-
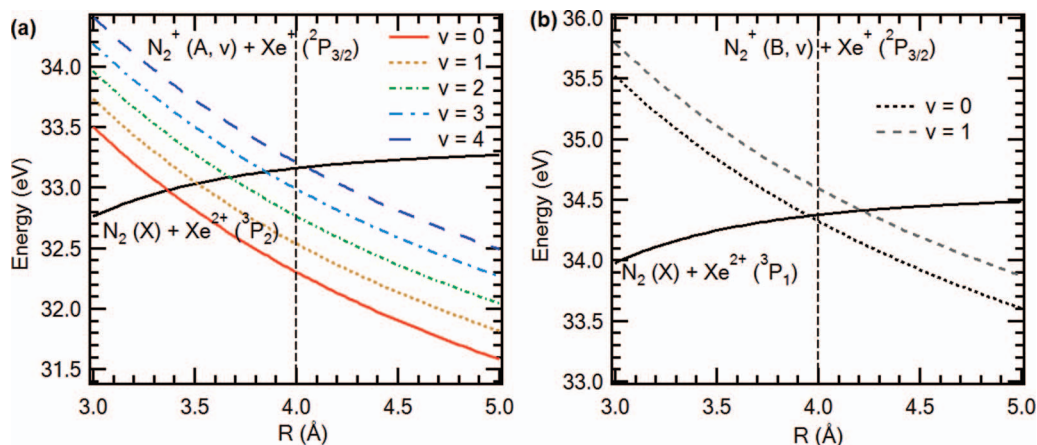
FIG. 10. (a) Vibronic curves of $Xe^{2+} + N_2$ charge-transfer reactant and Xe^+ ($^2P_{3/2}$) + N_2^+ (A) product states. (b) Same as (a) except for a spin-orbit excited reactant state, Xe^{2+} ($^2P_1$) + N_2, and Xe^+ ($^2P_{3/2}$) + N_2^+ (B) product states. The vertical line indicates optimal coupling near R = 4 Å.

cause vibrationally excited products have crossings at larger distances where the coupling is expected to be weaker, and because FC factors also favor $v = 0$ products. The low energy distributions, however, exhibit $v = 1$ populations that are slightly higher than those predicted by a Franck-Condon distribution (see Fig. 7). This implies that excited state reactants with crossings closer to the center of the charge-transfer crossing window are at play. Figure 10(b) depicts that spin-orbit excited $Xe^{2+}(^3P_1)$ + N_2 reactants, statistically representing about 30% of the beam, cross $Xe^+(^2P_{3/2})$ + N_2^+(B, $v = 0$) products very close to $R = 4$ Å. The preference for $v > 0$ states in comparison to a FC population implies that the optimal coupling occurs at larger distances than 4 Å. The larger integrated B state formation cross section compared to that of the A state products is consistent with an on average larger crossing radius. As for the A state product distribution, the distribution becomes more Franck-Condon with increasing collision energy (see Fig. 7(b)).

The present results, thus, exhibit at low energies state-to-state probabilities governed by a combination of an energy gap rule favoring states crossing near 4 Å and FC factors, and at high energies FC product state distributions. This trend has also been observed in previous charge-transfer luminescence studies of singly charged ions with molecules where the favored energy gap is closer to zero.[9,30,31] In those studies, the trend was associated with the increasing non-adiabaticity with translational energy that results in a broadening of the energy range of states that are coupled. This interpretation is in line with theoretical work on state-to-state charge-transfer dynamics.[6,10] Dressler et al.[30] distinguished between near-resonant vibrationally coupled product states that dominate at very low collision energies with state-to-state cross sections that decline with collision energy, and translationally coupled states whose state-to-state cross sections grow with collision energy. The vibrationally coupled states were interpreted to follow a vibronic curve-crossing mechanism along a Franck-Condon active vibrational coordinate orthogonal to the translational coordinate. The translational energy determines only the time interval (i.e., probability) during which an adiabatic traversal of the crossing seam on the multi-dimensional potential energy surface can occur. The translationally coupled

states on the other hand can be interpreted to follow a Rosen-Zener[32] or Demkov-type mechanism[33] in which near parallel (non-crossing) states are coupled through the motion along the interfragment coordinate. In such a mechanism, the transition probability approaches a maximum in the high energy limit, unlike the Landau-Zener CT probability which approaches zero. Thus, at the high energy limit, vibrationally coupled state-to-state probabilities are zero and the translationally coupled state-to-state probabilities have reached a maximum proportional to the FC factor of reactant and product vibrational wavefunctions.

Ehbrecht et al.[19] conducted luminescence studies of the doubly charged charge-transfer system, CO^{2+} + Ar, and also found a trend from non-FC distributions towards FC distributions in the high energy limit. Huber and Kahlert[34] conducted translational energy transfer measurements on the Xe^{2+} + H_2 system at low translational energies and found product distributions governed by a combination of energy gap and FC factors, similar to the present work. A closer look at the present results suggests that similar arguments applied to the interpretation of state-to-state dynamics of singly charge CT systems can be applied to the present doubly charged system that is dominated by a curve-crossing mechanism at low energies, and exhibits behavior suggesting a Rosen-Zener/Demkov type mechanism at higher energies. The energy dependence of the N_2^+(A) and N_2^+(B) state-to-state cross sections (Fig. 8, Tables II and III) suggest that the A state transitions, for which the cross sections increase with energy, are translationally coupled and the B state curve crossing, where the cross section decreases with energy, may involve vibrationally coupled transitions at the lowest energies for the lowest two N_2^+ product vibrational levels. The fact that the cross sections remain constant with energy at high energies is further support for a Rosen-Zener/Demkov over a Landau-Zener curve-crossing mechanism, where the CT probabilities are expected to decline with energy in the high energy limit.

The main difference in the present results compared with the singly charged studies is, thus, related to the energy gaps between asymptotic reactant and product states. As pointed out in previous studies,[16,19,34] the favored energy gap for doubly charged systems is related to the Coulomb energy at

the favored crossing distance of approximately 4 Å, which are significantly higher in the present system in comparison to those found for singly charged ion-molecule charge-transfer systems. This can be attributed to the much stronger long-range forces, in particular the product Coulomb potential, which shifts the regions of strong coupling with respect to the asymptotic reactant energy.

In summary, the present luminescence results of the Xe^{2+} + N$_2$ charge-transfer reaction are indicative of a long-range charge-transfer system. This is borne out by the weak energy dependence of the total electronic product state cross sections and the lack of rotational excitation in both the B-X and A-X emissions. The vibrational product state distributions are consistent with a curve-crossing model that assumes optimal electronic coupling near 4 Å. In contrast to singly charged systems where at low collision energies (<20 eV) product vibrational levels are preferred that adhere to the energy resonance criterion, the observed product Xe$^+$ + N$_2^+$ vibrational populations at low collision energies exhibit significant energy gaps with respect to the reactant energy and show a preference for vibrational product states with vibronic curve crossings in the vicinity of 4 Å. As observed in both singly and doubly charged systems, the populations approach a Franck-Condon distribution at the highest energies of this work, consistent with a pure translationally coupled mechanism of Rosen-Zener/Demkov type at high energies.

V. CONCLUSION

The ion-molecule reactions of Xe^{n+} + N$_2$ were monitored through single-collision chemiluminescence experiments at E$_{cm}$ = 4.5–211 eV for Xe$^+$ and 4.5–316 eV for Xe^{2+}. The Xe$^+$ + N$_2$ studies detect luminescence from excited nitrogen atoms above E$_{cm}$ = 20 eV. The luminescence is interpreted to be attributed to collision induced dissociation processes. Emission from xenon atoms provides some evidence for charge transfer, however, no N$_2^+$(A-X) or (B-X) radiance is detected. The Xe^{2+} + N$_2$ system is dominated by N$_2^+$ (A-X) and (B-X) transitions. The derived vibrational product state integrated emission excitation cross sections are found to be invariant over collision energies greater than 20 eV. The population of the vibrational states of N$_2^+$ (A) is seen to vary from a preference of $v = 3$ at low collision energies to nearing a FC distribution at high E$_{cm}$. The populations observed for both (A) and (B) states at low collision energies can be rationalized with a preference for electron transfer near 4 Å.

ACKNOWLEDGMENTS

[1]J. H. Moore and J. P. Doering, Phys. Rev. **177**, 218 (1969); G. H. Saban and T. F. Morgan, J. Chem. Phys. **57**, 895 (1972); L. G. Piper,

L. Gundel, J. E. Velazco, and D. W. Setser, J. Chem. Phys. **62**, 3883 (1975); D. Dhuicq, J. C. Brenot, and V. Sidis, J. Phys. B. **18**, 1395 (1985).

[2]T. R. Govers, M. Gérard, G. Mauclaire, and R. Marx, Chem. Phys. **23**, 411 (1977).

[3]C.-L. Liao, J.-D. Shao, R. Xu, G. D. Flesch, Y.-G. Li, and C. Y. Ng, J. Chem. Phys. **85**, 3874 (1986).

[4]G. Parlant and E. A. Gislason, J. Chem. Phys. **86**, 6183 (1987).

[5]*State-Selected and State-To-State Ion-Molecule Reaction Dynamics Part 1: Experiment*, edited by C.-Y. Ng and M. Baer (Wiley, New York, 1992), Vol. 82; *State-Selected and State-to-State Ion-Molecule Reaction Dynamics Part 2: Theory*, edited by M. Baer and C.-Y. Ng (Wiley, New York, 1992).

[6]E. A. Gislason, G. Parlant, and M. Sizun, "The semiclassical time-dependent approach to charge-transfer processes," in *Advances in Chemical Physics: State-Selected and State-To-State Ion Molecule Reaction Dynamics, Part 2. Theory,* edited by M. Baer and C.-Y. Ng (Wiley, New York, 1992), Vol. 82, pp. 321–421; V. Sidis, "Diabatic potential energy surfaces for charge-transfer processes," *ibid.*, pp. 73–134.

[7]C. Ottinger, in *Gas Phase Ion Chemistry*, Edited by M. T. Bowers (Academic, New York, 1984), Vol. 3, p. 249.

[8]J. J. Leventhal, in *Gas Phase Ion Chemistry*, edited by M. T. Bowers (Academic, New York, 1984), Vol. 3, p. 309.

[9]S. T. Arnold, R. A. Dressler, M. J. Bastian, J. A. Gardner, and E. Murad, J. Chem. Phys. **102**, 6110 (1995).

[10]E. A. Gislason and G. Parlant, Comments At. Mol. Phys. **19**, 157 (1987).

[11]R. A. Dressler, D. J. Levandier, S. Williams, and E. Murad, Comments At. Mol. Phys. **34**, 43 (1998).

[12]M. R. Spalburg and E. A. Gislason, Chem. Phys. **94**, 339 (1985); G.-H. Lin, J. Maier, and S. R. Leone, Chem. Phys. Lett. **125**, 557 (1986).

[13]A. L. Rockwood, S. L. Howard, W.-H. Du, P. Tosi, W. Lindinger, and J. H. Futrell, Chem. Phys. Lett. **114**, 486 (1985).

[14]N. G. Adams, D. Smith, and D. Grief, J. Phys. B **12**, 791 (1979).

[15]D. Smith, N. G. Adam, E. Alge, H. Villinger, and W. Lindinger, J. Phys. B **13**, 2787 (1980).

[16]W. Lindinger, Phys. Scr. **T3**, 115 (1983).

[17]Z. Herman, Int. Rev. Phys. Chem. **15**, 299 (1996).

[18]L. Landau, Physics of the Soviet Union **2**, 46 (1932); C. Zener, Proc. R. Soc. London, Ser. A **137**, 696 (1932).

[19]A. Ehbrecht, N. Mustafa, C. Ottinger, and H. Herman, J. Chem. Phys. **105**, 9833 (1996).

[20]Y.-h. Chiu, B. L. Austin, S. Williams, R. A. Dressler, and G. F. Karabadzhak, J. Appl. Phys. **99**, 113304 (2006).

[21]J. Sommerville, L. King, Y.-H. Chiu, and R. Dressler, J. Propul. Power **24**, 880 (2008).

[22]X. Tan, DIATOMIC a spectral simulation program for diatomic molecules on Windows platforms, release 1.28 (2004).

[23]K. P. Huber and G. Herzberg, "Constants of diatomic molecules," in *NIST Chemistry WebBook, NIST Standard Reference Database Number* 69, edited by P. J. Linstrom and W. G. Mallard, National Institute of Standards and Technology, Gaithersburg MD, 2010 20899, http://webbook.nist.gov.

[24]T. A. Miller, T. Suzuki, and E. Hirota, J. Chem. Phys. **80**, 4671 (1984).

[25]R. R. Laher and F. R. Gilmore, J. Phys. Chem. Ref. Data **20**, 685 (1991).

[26]C. Ottinger and J. Simonis, Chem. Phys. **28**, 97 (1978); G. Herzberg, *Molecular Spectra and Molecular Structure: Spectra of Diatomic Molecules* (Krieger, Malabar, FL, 1989), Vol. I.

[27]F. R. Gilmore, R. R. Laher, and P. J. Espy, J. Phys. Chem. Ref. Data **21**, 1005 (1992).

[28]Y. Ralchenko, A. E. Kramida, J. Reader, and NIST Atomic Spectra Database Team (2008) (National Institute of Standards and Technology, Gaithersburg, MD, 2008), Vol. 2010, http://www.nist.gov/pml/data/asd.cfm.

[29]Z. Herman, Phys. Essays **13**, 480 (2000)

[30]R. A. Dressler, S. T. Arnold, and E. Murad, J. Chem. Phys. **103**, 9989 (1995).

[31]T. Glenewinkel-Meyer and C. Ottinger, J. Chem. Phys. **100**, 1148 (1994).

[32]N. Rosen and C. Zener, Phys. Rev. **40**, 502 (1932).

[33]Y. U. Demkov, Sov. Phys. JETP **18**, 138 (1964).

[34]B. A. Huber and H-J. Kahlert, J. Phys. B **18**, 491 (1985).

DISTRIBUTION LIST

DTIC/OCP
8725 John J. Kingman Rd, Suite 0944
Ft Belvoir, VA 22060-6218   1 cy

AFRL/RVIL
Kirtland AFB, NM 87117-5776   2 cys

Official Record Copy
AFRL/RVBXT/Raymond Bemish   1 cy

This page intentionally left blank.